Termination of the 2018 Florida Red Tide Event: A Tracer Model Perspective

Yonggang Liu, Robert H. Weisberg, Lianyuan Zheng

College of Marine Science, University of South Florida, St. Petersburg, FL33701

Cynthia A. Heil

Mote Marine Laboratory, Sarasota, FL 34236

and

Katherine A. Hubbard

Florida Fish and Wildlife Conservation Commission- Fish and Wildlife Research Institute, St. Petersburg, FL 33701

6 May 2022

Corresponding author contact: Yonggang Liu, yliu@usf.edu

Final published version:

Liu, Y., Weisberg, R.H., Zheng, L., Heil, C.A., Hubbard, K.A. (2022), Termination of the 2018 Florida red tide event: A tracer model perspective, *Estuarine, Coastal and Shelf Science*, 272, 107901, https://doi.org/10.1016/j.ecss.2022.107901

Abstract

The 2018 *Karenia brevis* harmful algal bloom experienced along the west coast of Florida was the worst red tide occurrence there since 2005. Cell concentrations peaked in early fall of 2018, lessened in winter, and disappeared early in 2019. Here we examine the termination of this red tide event by using hindcast simulations of the West Florida Coastal Ocean Model, a numerical ocean circulation model that downscales from the deep Gulf of Mexico, across the continental shelf and into the estuaries. The underlying hypothesis is that without an offshore source of *K. brevis* cells, a nearshore bloom may quickly dissipate under the influence of a persistent upwelling circulation. To test this hypothesis, we used a passive tracer (without consideration of biological growth or decay) in the model to virtually indicate *K. brevis* cells. The tracer, inputted along the central West Florida coast where highest bloom concentrations were observed, was subsequently transported southward along the coast and offshore, significantly reducing the tracer concentrations over the three-month-long experimental duration, as was observed for the actual *K. brevis* cell concentrations. Whereas modeled tracer concentrations decreased over most of the West Florida coast, relatively higher concentrations remained just south of Sanibel Island, trapped there by the sharp bend in the coastline. Longer residence time for this area has important *K. brevis* implications. Lake Okeechobee nutrient flux through the Caloosahatchee River was thought to contribute to red tide in this region, and while these inputs may be a factor, a persistent upwelling circulation may also play a contributing role.

Keywords: Red tide, West Florida Shelf, tracer model, coastal upwelling, harmful algal bloom, bloom termination

1. Introduction

Blooms of the toxic dinoflagellate *Karenia brevis* (formerly *Gymnodinium breve*) occur frequently on the west coast of Florida (Steidinger, 1975), killing fish and other marine life, threatening public health and adversely impacting local economies throughout Florida (e.g., Anderson et al., 2021; Stumpf et al., 2022). Mitigating such effects requires improved forecast capabilities and hence better understanding of the mechanisms of red tide initiation, maintenance, and termination over the entire southwest Florida shelf region (e.g., Heil and Steidinger, 2009).

K. brevis bloom studies have an extensive background, with some 24 hypotheses on bloom initiation and growth reviewed by Vargo (2009). Many of the early thoughts of bloom initiation focused on the nearshore region, ascribing blooms to terrestrial nutrient sources associated with rainfall, runoff and ground water, with more recent examples including Hu et al. (2006), Brand and Compton (2007) and Medina et al. (2020). The concept of offshore initiation and shoreward advection were introduced by Steidinger (1975), and further documented by Steidinger and Haddad (1981) and Tester and Steidinger (1997). Weisberg et al. (2009a) provided a confirmation for such offshore initiation and shoreward advection for the 2005 *K. brevis* bloom. Hypotheses of bloom growth and maintenance necessarily involve a suite of complex biological and chemical processes to account for nutrient preferences and competition, growth rates, species competition and mortality (e.g., Liu et al., 2001; Mulholland et al., 2006; Vargo et al., 2008; O'Neil and Heil, 2014; Tilney et al., 2019). These disparate topics began to merge synergistically once interdisciplinary studies of *K. brevis* ramped up around 1998. In a seminal paper, Walsh et al. (2006) provided a process-oriented hypothesis of bloom initiation and development, whereby slow growing *K. brevis* can outcompete faster growing phytoplankton species in silicate deficient, oligotrophic waters by gaining nutrient support from nitrogen fixing *Trichodesmium* (Sipler et al. 2013; Mulholland et al. 2014), whose growth is facilitated by iron-rich Saharan dust (Lenes et al., 2001, 2008). Once the bloom reaches sufficient concentration to dominate the phytoplankton community, it can utilize all available nutrient sources as well as generating its own nutrient supply by utilizing *K. brevis* toxins to kill fish (Walsh et al., 2009; Heil et al 2014).

Whether or not the offshore nutrient state is conducive for *K. brevis* outcompeting other species may depend on the circulation. This hypothesis was demonstrated by the companion papers of Weisberg and He (2003) and Walsh et al. (2003). The first of these, using observations and a realistic numerical circulation model simulation for the spring and summer seasons of 1998, showed how the Gulf of Mexico Loop Current, when contacting the shelf slope near the Dry Tortugas, set the entire West Florida Shelf (WFS) in an upwelling favorable motion, resulting in the transport of deeper, nutrient-rich waters across the shelf break and shoreward within the bottom Ekman layer. Using the velocity field from the first to drive an ecological model, the second of these accounted for the observed nutrient (nitrate) and phytoplankton (mostly diatoms) distributions offshore as observed in spring and summer 1998.

These concepts of how the WFS circulation may give rise to inter-annual variability in *K. brevis* bloom intensity were further advanced by Weisberg et al. (2014a), who explained why there was no *K. brevis* bloom in 2010 and by Weisberg et al. (2016b) who compared the relatively pronounced, versus sedate *K. brevis* blooms of 2012 and 2013. In essence, the ocean circulation physics were found to be as important for *K. brevis* ecology as the organism biology. Expanding on these ideas, Liu et al. (2016), through a joint analysis of *K. brevis* cell counts and Loop Current evolution (via satellite altimetry) developed a seasonal prediction scheme for major red tide occurrences (or lack thereof) that was successful in 22 out of 25 years, including the 2018 major red tide event (Weisberg et al., 2019).

Compared with *K. brevis* bloom initiation and development studies, there are fewer studies regarding bloom termination. Biological processes potentially contributing to *K. brevis* bloom termination studies that have been studied include grazing from macrozooplankton (e.g., Speekmann et al., 2006; Breier and Buskey, 2007), zooplankton (e.g., Dagg, 1995; Sutton et al., 2001) and microzooplankton (e.g., Kubanek et al., 2007), lysis from bacterial and/or viral cells (e.g., Paul et al., 2002; Brussaard, 2004; Mayali and Doucette, 2002; Lenes et al., 2013; Patin et al., 2020) and nutrient depletion (Vargo, 2009). Recently, mechanisms of *K. brevis* intrinsic cell loss/death processes have also been investigated with lab experiments (Gao and Erdner, 2022). However, it remains unclear how these complex biological processes may play a role in terminating *K. brevis* blooms on the WFS. Physical processes were suggested to be important for bloom termination by Tester et al. (1991), and transport of *K. brevis* cells from the WFS to the east Florida coast was documented by Tester and Steidinger (1997), Walsh et al. (2009) and Harris et al. (2020). However, no specific studies examining the role of physical processes in termination of blooms presently exist.

The 2018 *K. brevis* bloom was the most environmentally destructive harmful algal bloom (HAB) on the west Florida coast in more than a decade. It started quite normally in late-summer/fall of 2017, but then persisted through the winter and subsequent spring, with cell concentrations at high levels (cell counts > 10^6 cells/L) southward from Venice, Florida through January 2019. Based on the Liu et al. (2016) “pressure point” prediction scheme, the ocean circulation conditions for 2018 were predicted to be conducive for further offshore development of a new *K. brevis* bloom. The summer of 2018 saw a change in the Loop Current state from one in which the Loop Current penetrated far into the Gulf of Mexico to one in which it retreated back to a more direct inflow outflow state with "pressure point" contact. Whereas this state change occurred too late to mitigate offshore *K. brevis* development in 2018, once the contact occurred in July of 2018, it ensured that what was growing offshore would be transported to the nearshore by the induced upwelling circulation. Consequently, the newly formed 2018 bloom combined together with the existing overwintering 2017 bloom, setting the stage for a persistent and spatially extensive *K. brevis* bloom that lasted through 2018 and into the beginning of 2019. Thus, the coastal ocean circulation played an important role in accounting for the outbreak and intensity of the 2018 bloom (Weisberg et al., 2019).

The present work continues the study of the 2017-2019 *K. brevis* bloom event with a focus on the bloom termination. The same numerical model, the West Florida Coastal Ocean Model (WFCOM, Zheng and Weisberg, 2012 and Weisberg et al, 2014b), will be employed here. Different from the applications in Weisberg et al. (2019), which were based on Lagrangian trajectory simulations, the WFCOM with an embedded tracer module is used here instead. The purpose is to investigate how a passive tracer, originating nearshore, may be transported and dissipated by advection and turbulent diffusion, independent of biological or chemical interactions once the tracer source abates. In other words, it examines whether or not the circulation can account for *K. brevis* bloom termination under certain conditions.

Note that this WFCOM application is built on top of a series of previous efforts in setting up a proper numerical ocean circulation model for the WFS. A brief review of the relevant modeling work is provided in Section 2, along with the WFCOM settings and the implementation of the tracer model experiment. Model results are analyzed in Section 3, followed by summary and discussion in Section 4.

2. Methods

2.1. A brief review of the West Florida Coastal Ocean Model

Modeling the WFS circulation requires the inclusion of both local (winds, heat and fresh water fluxes) and deep-ocean forcing (e.g., Weisberg and He, 2003; Weisberg and Liu, 2022). Thus, the WFCOM was designed to downscale from the deep ocean, across the continental shelf and into the estuaries (Zheng and Weisberg, 2012; Weisberg et al., 2014b). The unstructured grid, Finite Volume Community Ocean Model (FVCOM), developed by University of Massachusetts Dartmouth (Chen et al., 2003), was chosen to allow for increasing resolution upon approaching the coast and entering the various estuary inlets. This avoids multiple nesting procedure that is usually required to down scale from a low resolution regional ocean model to a high resolution estuary model. Also, the high resolution triangular grid can better resolve the complicated coastlines. FVCOM, through its many applications (e.g., Hu et al., 2008; Xia et al., 2020), is an established coastal ocean model. To include forcing from the deep ocean, WFCOM nests in the Hybrid Coordinate Ocean Model (HYCOM; e.g., Chassignet et al., 2009). The original application, documented by Zheng and Weisberg (2012), extended landward from about the 200 m isobath and covered a domain from the Desoto Canyon (Pensacola, FL) region in the northwest to just south of the Florida Keys. Recognizing the need to have real time Mississippi River inflows (versus climatology), WFCOM was subsequently modified to extent westward of the Atchafalaya Basin and to nest in the Gulf of Mexico (GOM) HYCOM (e.g., Zamudio and Hogan 2008; Halliwell et al., 2009), which includes tides. The domain of this present version is provided in Figure 1, and an initial application is given by Weisberg et al. (2014b). With its 65,435 nodes and 125,357 triangular elements, WFCOM presently has a horizontal resolution that increases toward the coast from ~12 km at the open boundary to ~150 m in the estuaries. Vertically, the model has 31 sigma layers with higher resolution near the surface and bottom to better resolve the Ekman layers. Surface forcing includes momentum and heat fluxes interpolated from the NOAA NCEP North American Mesoscale Forecast System (NAM) that are served via NOAA Operational Model Archive and Distribution System (NOMADS). WFCOM is one-way nested within the GOM HYCOM. Nesting includes sea surface elevation, 2D and 3D velocity components, inclusive of tides, as well as 3D temperature and salinity, all within with a buffer zone consisting of 10 nodes over which the weighting function varies linearly from 1 to zero. River inflows are added as daily mean river discharges, downloaded from the US Geological Survey (USGS) and South Florida Water Management District (SFWMD) web servers. We also note that WFCOM includes a flooding and drying capability that is essential for simulating scalar concentrations in shallow water that may either dry or result in coastal inundation under strong wind conditions (e.g., Chen et al. 2008a, 2013).

Numerous applications over the past decade, each with model/observation comparisons, demonstrate WFCOM's utility in simulating circulation and water property variations of interdisciplinary concern. The first of these (Zheng and Weisberg, 2012) evaluated the performance of the original WFCOM using in situ time series of velocity, temperature and salinity from WFS moorings for calendar year 2007. WFCOM was found to reproduce the circulation and water mass variations reasonably well over this year-long simulation. Spring, 2007 was particularly interesting because it contained a period of time when the Loop Current was in contact with the southwest corner of the WFS, later termed the pressure point by Liu et al. (2016). As hypothesized by Hetland et al. (1999) and confirmed by Weisberg and He (2003), the Loop Current when in contact there may set the entire WFS in an upwelling favorable motion.

This 2007 event, when coupled with gag grouper juvenile observations, enabled Weisberg et al. (2014b) to solve the gag grouper recruitment conundrum of how larvae, originating at shelf break spawning sites, can arrive at their nearshore and estuarine settlement sites. Several applications of WFCOM to the Deepwater Horizon oil spill event are also notable. Liu et al. (2014) tested the WFCOM simulations using satellite-tracked surface drifter observations during summer 2010 and found the WFCOM had better performance on the WFS than the other models. The question of whether or not Deepwater Horizon hydrocarbons transited to the WFS to account for reef fish lesions found there was addressed by Weisberg et al. (2016c) using a simulated tracer deployed along the northern Gulf coast, where oil was observed to have covered the surface. Weisberg et al. (2017) then used WFCOM to explain how Deepwater Horizon oil arrived on northern Gulf beaches via combination of advection and wave-induced Stokes drift. With regard to the coastal ocean circulation and storm surge response to hurricanes, Liu et al. (2020) compared the WFCOM simulated current velocity with the moored observations at three real-time data buoys on the WFS, and found that the model successfully reproduced the shelf circulation response to Hurricane Irma. The comparisons between simulated and observed sea levels at various coastal tide gauge stations along the west Florida coast were generally good, capturing the initial set downs and subsequent rises of sea levels in Florida Bay and in the estuaries as Hurricane Irma transited northward along the Florida peninsula. All these studies demonstrate fidelity when using WFCOM for a variety of interdisciplinary coastal ocean applications.

WFCOM applications to *K. brevis* HABs are also notable. Along with the oil spill, 2010 was a year when no bloom event was observed on the WFS. Weisberg et al. (2016a) explained this on the basis of new inorganic nutrients having been upwelled onto the WFS by the persistent upwelling that occurred beginning in May of that year. By abundant upwelled nutrients supporting fast growing phytoplankton species offshore at depth at the expense of slower growing *K. brevis*, we may account for the lack of a red tide. As in the prior studies mentioned above, several time series from WFS moorings, along with data from a glider transect, provided veracity testing. These concepts led to an Occam's Razor approach to *K. brevis* seasonal forecasts (Liu et al., 2016) that was found to be correct for 17 out of 22 years for which joint circulation (via satellite altimetry) and *K. brevis* cell count data were available. Weisberg et al. (2016b) also used WFCOM simulations, moored velocity data and glider data to explain why the 2012 red tide was more pronounced than the nominal 2013 event. With the circulation now recognized as being an important contributor to *K. brevis* HABs, and in collaboration with Fish and Wildlife Research Institute (FWRI) colleagues, daily, automated red tide trajectory forecasts are now served to the general public and agency personnel at: http://ocgweb.marine.usf.edu/hab_tracking/. FWRI provides cell counts and WFCOM is used to project these forward in time and space over a 4.5 day interval. Such short-term forecasts were particularly useful to help guide clean-up operations throughout the 2018 *K. brevis* event, and subsequent WFCOM hindcasts enabled us to explain why the event was so intense and why *K. brevis* cells were also simultaneously found along the west coast of Florida, the Florida Panhandle and Florida's east coast (Weisberg et al., 2019).

2.2. Tracer model experiment

FVCOM includes a dye module that simulates tracer concentration variations by advection and diffusion. The tracer serves as a virtual marker of the water mass in the model domain. It is transported from one place to another by advection and diluted through mixing with ambient water. The dye module conserves tracer mass by using a flux calculation of second-order accuracy to avoid numerical tracer loss (Chen et al., 2008b). Several applications exist in the literature. As examples, Weisberg (2011) adopted it for simulating the flushing of a residential channel under the action of tides and winds. Lai et al. (2013) used it in tracking the radionuclide that flowed out of the Fukushima nuclear power plant. Zhu et al. (2015) applied it in a study of the flushing processes in the Tampa Bay. Weisberg et al. (2016c) employed the virtual tracer for examining the transport of the Deepwater Horizon hydrocarbons to the WFS. Here we use the FVCOM tracer module to study the role of advection and diffusion in terminating the 2018 red tide event, independent of more complex, and largely unknown, biological processes.

The protracted 2017-2019 *K. brevis* red tide peaked from summer to fall 2018 with sustained cell concentrations exceeding 10^6 cells per liter from September through November (**Figure 2**). Highest concentrations were located along the central WFS coast between Tampa Bay to Charlotte Harbor, attributed to the advection and concentration of new cells advected there from offshore into this region. Lesser regions of *K. brevis* were also found along the Florida Panhandle coast and the Florida east coast, also due to the transport by the ocean currents (Weisberg et al., 2019). Given this evolution, what might happen once the supply of new cells from offshore ceases? To address this question, we released a passive tracer in a coastal zone from latitudes of Tampa Bay to Naples, Florida. The release was limited to a narrow band along the 10 m isobath to the coast (**Figure 1**). Thus, all of the grid nodes within this area were initialized uniformly throughout the water column (i.e., in all the 30 σ layers) with a normalized concentration of 1, whereas all of the other nodes in the WFCOM domain were initialized with a tracer concentration of zero. This initial tracer concentration started at 0000 UTC on 1 October

2018, and the tracer concentration experiment was run online as part of a realistic circulation hindcast simulation for the four-month interval: 1 October – 31 December 2018.

3. Results

3.1. Coastal upwelling circulation

The circulation on the inner WFS is mostly wind-driven due to its wide and gently sloping bottom and semi-enclosed coastline (**Figure 1**). The long-term mean circulation is upwelling, with seasonal and synoptic weather band variations as determined from the multiple-year record of moored velocity data (Weisberg et al., 2009b; Liu and Weisberg, 2005, 2007, 2012). The period of October – December corresponds to the fall and winter seasons, and the coastal ocean circulation is predominantly in upwelling patterns, i.e., the currents are generally directed down-shelf (southeastward) with an offshore component in the surface currents and onshore component near the bottom, resulting in an upwelling near the coast due to continuity of the water. This fall-winter upwelling circulation tends to transport coastal materials in the down-shelf direction and spreads them away from the coast near the surface.

To better illustrate the coastal upwelling current structures, we use the WFCOM output on 13 October 2018 as an example. The daily averaged currents are interpolated from the FVCOM native unstructured grid to a coarser, rectangular mesh for better visualization, and the velocities in the top-most and bottom-most sigma layers are shown as near surface and near bottom currents, respectively (**Figure 3**). In both near surface and bottom layers, the currents were oriented in the down-shelf direction over the inner WFS. The surface currents were southward or southwestward (with an offshore component), with a stronger velocity (maximum 30 – 40 cm/s), while the near-bottom currents were weaker (maximum 10 – 20 cm/s) and southeastward (with an onshore component). From surface down to bottom, the current vector veered to the left over the inner shelf. To further explore the vertical structure of the coastal currents, we show the daily averaged velocity and salinity on the same day (13 October 2018) along a transect across the WFS offshore from Sarasota, Florida. There was a strong coastal upwelling jet with a core (maximum along-shelf velocity > 34 cm/s) at subsurface level between the 50 m and 60 m isobaths, which was accompanied by fully developed bottom Ekman layer with the positive/onshore across-shelf velocity component in the near bottom 10 – 15 m layer and a surface Ekman layer with the negative/offshore across-shelf velocity component in the top 10 – 20 m layer (**Figure 4**). The onshore velocity component extended from 130 km offshore all the way to the coast, with the strongest onshore flow just below the core of the coastal upwelling jet. As a result, the near-bottom water was upwelled onto the inner shelf and near the coast, which is evidenced by the nook of salinity contours near the bottom (higher salinity water was upwelled and mixed with the coastal fresher water). Similarly, surface water was advected away from the coast, which can also be seen from the salinity contours that tend to lean towards offshore in the near surface layer except for the very shallow water area (water depth <10 m). The coastal upwelling circulation system transported the coastal materials (the tracer or *K. brevis* cells here in this study) down the shelf (southeastward) and spread them offshore. By mixing with deeper water column offshore, the concentration of the materials decreased quickly when advected away from the coast.

3.2. Tracer advection and dissipation

Snapshots of WFCOM-simulated surface tracer concentration for the WFS coastal region from Tampa Bay to the Florida Keys at various time intervals (three days, one week, two weeks, and then from one to three months) after initialization are shown in **Figure 5**. With no new tracer added after the first model time step, we see that the tracer concentration quickly decreases nearshore. Thus, if the offshore source abates, then the same upwelling circulation that would have brought new tracer to the shoreline now acts to rid the shoreline of what was initially there. This is particularly evident at the mouths of the Tampa Bay and Charlotte Harbor estuaries where strong tidal currents hasten the flushing of the tracer from these locations. The upper-left hand panel shows that within three days of the tracer release (by 4 October 2018), the tracer concentration is decreased by more than 50% near these two estuarine tidal inlets (**Figure 5a**). Given the persistent upwelling circulation that existed from October to January, the tracer is advected southward along the coast, with steamers extending offshore, resulting in a reduction of the concentration with time. By the end of October 2018 (one month after the tracer release), the normalized tracer concentration was reduced by 70% to 80% (from 1 to 0.2~0.3) for most areas of the coastal region from Tampa Bay to Naples. By the end of November 2018 (two months after the tracer release), the northern half of the original tracer patch was transported to the south and further dissipated, and by the end of the third month (December 2018), the tracer all but disappeared with the exception of the region between from Sanibel Island to the Florida Keys, with much reduced concentration.

The lower panel of **Figure 5** shows time series of surface tracer concentration sampled at five locations along the WFS, as indicated in the figure insert, i.e., from north to south, near Clearwater, the Tampa Bay mouth, the Charlotte Harbor mouth, Sanibel Island, and Naples. There was rapid reduction of the tracer concentration during the first several days near the Charlotte Harbor inlet. Within about three weeks of the tracer release, the tracer concentration offshore off Clearwater was reduced by 90%, and those near Naples and the mouths of Tampa Bay and Charlotte Harbor were also largely decreased, by 60% to 80%. The slowest reduction was located just south of Sanibel Island, where the normalized tracer concentration remained above 0.4 until 40 days after the tracer release.

The Sanibel Island to the Ft. Meyers Beach area includes a sharp bend to the coastline (**Figure 1**) that tends to trap tracer in its lee under the influence of an upwelling circulation. Thus, the tracer tended to accumulate in this region and farther down coast to the Naples vicinity, as shown by the enlargements of **Figure 6**. The region of highest tracer concentration was located within the coastline nook, with a peak value of 0.6 and above even one month after release (**Figure 6c**). Such relatively higher tracer concentration was in place on 30 November 2021, two months after the tracer release (**Figure 6d**). Some of the tracer even entered the Charlotte Harbor estuary behind Sanibel Island, and was maintained in place there through 31 December 2018, more than three months after the release (**Figure 6e**). From this we may surmise that abrupt changes in coastline configuration and orientation are important in determining the distribution of HABs. This is consistent with findings by Picher et al. (2010) who considered an array of coastline configurations, including headlands, capes, peninsulas, bays and estuaries, representing regions of increasing isolation and consequently regions of increased retention times for HABs.

Whereas the above discussion focused upon surface concentrations (in the top sigma layer), given the shallowness of the nearshore, the near bottom concentrations (in the bottom sigma layer) are very similar to the surface ones (the lower panels **Figures 6g** through **6l**). Small differences between the surface and bottom tracer concentration are mainly seen in the deeper waters offshore of the 10 m isobath, where surface tracer was spread offshore and further diluted relative to the bottom tracer that tended to hug the coast consistent with the upwelling circulation.

4. Discussion and Conclusions

We examined the termination process of the 2017-2019 Florida *K. brevis* HAB event using a passive tracer deployed in our West Florida Coastal Ocean Model, that was previously shown to provide a realistic hindcast of the coastal ocean circulation for this event (Weisberg et al., 2019). We hypothesized that the same persistent upwelling circulation that supports the advection of an offshore source of red tide to the coast within the bottom Ekman layer, would act to reduce red tide cell concentrations by advection and diffusion once the source of cells was reduced, independent of biological processes or chemical interactions that are largely unknown or lack definite relationships with *K. brevis* cell death/decay. To test this hypothesis, a band of conservative tracer was released (and abruptly stopped) along the coast line between the shore and the 10 m isobath. Without replenishment by new tracer from farther offshore, the tracer concentration quickly decreased by advection and diffusion, particularly near Tampa Bay and Charlotte Harbor estuary mouths where strong tidal currents add to the upwelling circulation. Thus, under the upwelling conditions, the tracer was advected southward along the coast, with steamers dissipating offshore, resulting in a reduction of the concentration over time. Independent of biological growth or decay processes, the upwelling circulation resulted in a substantial reduction in tracer concentration over the three-month period. This simplistic experiment demonstrated that *K. brevis* blooms, initiated offshore and transported to the nearshore along the bottom, can quickly manifest as high concentration blooms along the coastline, but that once the offshore source of cells is cut off, then the circulation can quickly cause bloom concentrations to decrease. Thus we may conclude that the same physical oceanographic processes that play an important role in initiating a *K. brevis* bloom may also account for bloom termination, as demonstrated for the 2017-2019 west Florida *K. brevis* HAB.

Additionally, it was found that due to the coastline geometry, an upwelling favorable circulation may trap *K. brevis* cells (or other materials) within the coastline nook just south from Sanibel Island. Whereas nutrient flux of terrestrial and upland origin (i.e., via the Caloosahatchee River draining Lake Okeechobee) is often argued as being related to *K. brevis* in that area (e.g., Medina et al., 2020), the longer residence time of this region suggests that *K. brevis* accumulation there may also be due to a combination of local hydrography and generation and transport of cells from elsewhere. This interesting finding was obtained through the numerical model experiment, a convenient way to examine the coastal ocean processes. Future in situ observations are warranted to ascertain whether this offshore source is an important contributor to the local red tide.

Acknowledgments:

Support was provided by the NOAA ECOHAB program (award NA19NOS4780183), NOAA/IOOS through the Southeast Coastal Ocean Observing Regional Association (SECOORA, award NA21NOS0120097), NOAA Office of Coast Survey through the Center for Ocean Mapping and Innovative Technologies (COMIT, award NA20NOS4000227), the State of Florida through FWC/FWRI (agreement # 20035) and the USF COMPS program. This work benefited from the Extreme Science and Engineering Discovery Environment (XSEDE, award OCE170007), which is supported by National Science Foundation grant ACI-1548562 (Towns et al., 2014). This is NOAA ECOHAB Publication # 1019.

References:

Anderson, D.M., Fensin, E., Gobler, C.J., Hoeglund, A.E., Hubbard, K.A., Kulis, D.M., Landsberg, J.H., Lefebvre, K.A., Provoost, P., Richlen, M.L., Smith, J.L., Solow, A.R., Trainer, V.L. (2021). Marine harmful algal blooms (HABs) in the United States: history, current status and future trends. *Harmful Algae* 102, 101975.

Brand, L.E., & Compton, A. (2007). Long-term increase in *Karenia brevis* abundance along the Southwest Florida Coast. *Harmful Algae* 6, 232-252.

Breier, C.F., & Buskey, E.J. (2007). Effects of the red tide dinoflagellate, *Karenia brevis*, on grazing and fecundity in the copepod Acartia tonsa. *J. Plankton Res*. 29, 115–126.

Brussaard, C.P.D. (2004). Viral control of phytoplankton populations—a review. *J. Eukaryot. Microbiol.* 51, 125–138.

Chassignet, E. P., Hurlburt, H. E., Metzger, E. J., Smedstad, O. M., Cummings, J., Halliwell, G. R., et al. (2009). U.S. GODAE: Global Ocean Prediction with the HYbrid Coordinate Ocean Model (HYCOM). *Oceanography* 22, 48–59.

Chen, C. S., Liu, H., & Beardsley, R. C. (2003). An unstructured, finite-volume, three-dimensional, primitive equation ocean model: Application to coastal ocean and estuaries. *J. Atmos. Oceanic Technol*. 20(1), 159–186.

Chen, C., Qi, J., Li, C., Beardsley, R.C., Lin, H., Walker R., & Gates, K. (2008a). Complexity of the flooding/drying process in an estuarine tidal-creek salt-marsh system: an application of FVCOM. *J. Geophys. Res*. 113, C07052, doi:10.1029/2007JC004328.

Chen, C.S., Xu, Q., Houghton, R., & Beardsley, R.C. (2008b). A model-dye comparison experiment in the tidal mixing front zone on the southern flank of Georges Bank. *J. Geophys. Res.* 113, C02005, doi:10.1029/2007jc004106.

Chen, C., R.C. Beardsley, R.A. Luettich Jr., et al. (2013). Extratropical storm inundation testbed: intermodel comparisons in Scituate, Massachusetts. *J. Geophys. Res. Oceans* 118, 5054–5073, doi:10.1002/jgrc.20397.

Dagg, M.J. (1995). Copepod grazing and the fate of phytoplankton in the northern Gulf of Mexico. *Con. Shelf Res*. 15, 1303–1317.

Gao, Y., & Erdner, D.L. (2022). Dynamics of cell death across growth stages and the diel cycle in the dinoflagellate *Karenia brevis*. *J. Eukaryot. Microbiol.* 69, e12874, doi:10.1111/jeu.12874.

Halliwell, G.R., Jr., A. Barth, R.H. Weisberg, et al. (2009). Impact of GODAE products on nested HYCOM simulations on the west Florida shelf. *Ocean Dynamics* 59 (1), 139–155.

Harris R.J., Arrington D.A., Porter D., & Lovko V. (2020). Documenting the duration and chlorophyll pigments of an allochthonous *Karenia brevis* bloom in the Loxahatchee River Estuary (LRE), Florida. *Harmful Algae* 97, 101851, doi:10.1016/j.hal.2020.101851.

Heil, C.A., Dixon, L.K., Hall, E., Garrett, M., Lenes, J.M., O'Neil, J.M., Walsh, B.M., Bronk, D.A., Killberg-Thoreson, L., Hitchcock, G.L., Meyer, K.A. (2014). Blooms of *Karenia brevis* (Davis) G. Hansen & Ø. Moestrup on the West Florida Shelf: Nutrient sources and potential management strategies based on a multi-year regional study. *Harmful Algae 38*, 127–140, doi:10.1016/j.hal.2014.07.016.

Heil, C.A., Steidinger, K.A. (2009). Monitoring, management, and mitigation of *Karenia* blooms in the eastern Gulf of Mexico. *Harmful Algae* 8, 611-617.

Hetland, R.D., Hsueh, Y., Leben, R., & Niller, P. (1999). A loop current induced jet along the edge of the west Florida shelf. *Geophys. Res. Lett.* 26, 2239–2242.

Hu, C., Muller-Karger, F. E., & Swarzenski, P. W. (2006). Hurricanes, submarine groundwater discharge, and Florida's red tides. *Geophys. Res. Lett.* 33, L11601, doi:10.1029/2005GL025449

Hu, S., Townsend, D.W., Chen, C., Cowles, G., Beardsley, R.C., Ji, R., Houghton, R.W. (2008). Tidal pumping and nutrient fluxes on Georges Bank: A process-oriented modeling study. *J. Mar. Sys.* 74, 528-544, doi:10.1016/j.jmarsys.2008.04.007.

Kubanek, J., Snell, T.W., & Pirkle, C. (2007). Chemical defense of the red tide dinoflagellate *Karenia brevis* against rotifer grazing. *Limnol. Oceanogr*. 52, 1026–1035.

Lai, Z., Chen, C., Beardsley, R., Lin, H., Ji, R,. Sasaki, J., & Lin J. (2013). Initial spread of ^{137}Cs from the Fukushima Dai-ichi Nuclear Power Plant over the Japan continental shelf: a study using high-resolution, global-coastal nested ocean model. *Biogeosciences* 10, 5439–5449.

Lenes, J.M., Darrow B.P., Cattrall, C., Heil, C.A., et al. (2001). Iron fertilization and the *Trichodesmium* response on the west Florida shelf. *Limnol. Oceanogr*. 46, 1261–1277.

Lenes J.M., Darrow B.P., Walsh J.J., Prospero J.M., et al. (2008). Saharan dust and phosphatic fidelity: a 3 dimensional biogeochemical model of Trichodesmium as a nutrient source for red tides on the West Florida shelf. *Cont. Shelf Res.* 28, 1091−1115.

Lenes, J.M., Walsh, J.J., Darrow, B.P. (2013). Simulating cell death in the termination of *Karenia brevis* blooms: implications for predicting aerosol toxicity vectors to humans. *Mar. Ecol. Prog. Ser.* 493, 71–81. doi:10.3354/meps10515.

Liu, G., Janowitz, G.S., & Kamykowski, D. (2001). A biophysical model of population dynamics of the autotrophic dinoflagellate *Gymnodinium breve*. *Mar. Ecol. Prog. Sers*. 210, 101-124.

Liu, Y., & Weisberg, R.H. (2005). Patterns of ocean current variability on the West Florida Shelf using the self-organizing map. *J. Geophys. Res. Oceans* 110, C06003, doi:10.1029/2004JC002786.

Liu, Y., & Weisberg R.H. (2007). Ocean currents and sea surface heights estimated across the West Florida Shelf. *J. Phys. Oceanogr.* 37(6), 1697-1713, doi:10.1175/JPO3083.1.

Liu, Y., & Weisberg R.H. (2012). Seasonal variability on the West Florida Shelf. *Progr. Oceanogr*. 104, 80-98, doi:10.1016/j.pocean.2012.06.001.

Liu, Y., Weisberg, R.H., Vignudelli, S., & Mitchum, G.T. (2014). Evaluation of altimetry-derived surface current products using Lagrangian drifter trajectories in the eastern Gulf of Mexico. *J. Geophys. Res. Oceans* 119: 2827–2842, doi:10.1002/2013JC009710.

Liu, Y., Weisberg, R.H., Lenes, J., Zheng, L., Hubbard, K., & Walsh, J.J. (2016). Offshore forcing on the West Florida shelf "pressure point" and its upwelling influence on harmful algal blooms. *J. Geophys. Res. Oceans 121*, 5501–5515, doi:10.1002/2016JC011938

Liu, Y., Weisberg, R.H., & Zheng, L. (2020). Impacts of hurricane Irma on the circulation and transport in Florida Bay and the Charlotte Harbor estuary. *Estuaries and Coasts* 43, 1194-1216, doi:10.1007/s12237-019-00647-6.

Mayali, X., & Doucette, G.J. (2002). Microbial community interactions and population dynamics of an algicidal bacterium active against *Karenia brevis* (Dinophyceae). *Harmful Algae* 1, 277–293.

Medina, M. Huffaker, R., Jawitz, J.W., & Muñoz-Carpena, R. (2020). Seasonal dynamics of terrestrially sourced nitrogen influenced *Karenia brevis* blooms off Florida's southern Gulf Coast. *Harmful Algae* 98, 101900, doi:10.1016/j.hal.2020.101900.

Mulholland, M. R., Bernhardt, P. W., Heil, C. A., Bronk, D.A., & Neil, J.M.O. (2006). Nitrogen fixation and release of fixed nitrogen by *Trichodesmium spp*. in the Gulf of Mexico. *Limnol. Oceanogr.* 51, 1762–1776. doi:10.4319/lo.2006.51.4.1762.

Mulholland, M. R., Bernhardt, P. W., Ozmon, I., Procise, L. A., Garrett, M., O'Neil, J. M., Heil, C. A., Bronk, D. A. (2014). Contribution of diazotrophy to nitrogen inputs supporting *Karenia brevia* blooms in the Gulf of Mexico. *Harmful Algae* 38, 20–29, doi:10.1016/j.hal.2014.04.004.

O'Neil, J. M., & Heil, C. A. (Eds.) (2014). Nutrient dynamics of *Karenia brevis* red tide blooms in the eastern Gulf of Mexico. *Harmful Algae 38*, 1–140.

Patin, N.V., Brown, E., Chebli, G., Garfield, C., Kubanek, J., & Stewart, F.J. (2020). Microbial and chemical dynamics of a toxic dinoflagellate bloom. *PeerJ* 8:e9493, doi:10.7717/peerj.9493.

Paul, J.P., Houchin, L., Griffin, D., Slifko, T., Guo, M., Richardson, B., & Steidinger, K. (2002). A filterable lytic agent obtained from a red tide bloom that caused lysis of *Karenia brevis* (Gymnodinium breve) cultures. *Aq. Microb. Ecol*. 27, 21–27.

Pitcher, G.C., Figueiras, F.G., Hickey, B.M., & Moita, M.T. (2010). The physical oceanography of upwelling systems and the development of harmful algal blooms. *Prog Oceanogr*. 85(1-2), 5–32, doi:10.1016/j.pocean.2010.02.002.

Sipler, R.E., Bronk, D.A., Seitzinger, S.P., Lauck, R.J., McGuinness, L.R., Kirkpatrick, G.J., Heil, C.A., Kerkhof, L.J. and Schofield, O.M. (2013). Trichodesmium-derived dissolved organic matter is a source of nitrogen capable of supporting the growth of toxic red tide *Karenia brevis*. *Marine ecology progress series*, *483*, 31-45.

Speekmann, C.L., Hyatt, C.J., & Buskey, E.J. (2006). Effects of *Karenia brevis* diet on RNA:DNA ratios and egg production of Acartia tonsa. *Harmful Algae* 5, 693–704.

Steidinger, K. A. (1975). Implications of dinoflagellate life cycles on initiation of *Gymnodinium breve* red tides. *Environmental Letters 9*(2), 129–139, doi:10.1080/00139307509435842.

Steidinger, K.A., & Haddad, K. (1981). Biologic and hydrographic aspects of red tides. *Bioscience* 31, 814-819.

Stumpf, R.P., Li ,Y., Kirkpatrick, B., Litaker, R.W., Hubbard, K.A., Currier, R.D., et al. (2022). Quantifying *Karenia brevis* bloom severity and respiratory irritation impact along the shoreline of Southwest Florida. *PLoS ONE* 17(1): e0260755, doi:10.1371/journal.pone.0260755.

Sutton, T.T., Hopkins, T.L., Remsen, A.W., & Burghart, S.E. (2001). Multisensor sampling of pelagic ecosystem variables in a coastal environment to estimate zooplankton grazing impact. *Cont. Shelf Res*. 21, 69–87.

Tester, P.A., & Steidinger, K.A. (1997). *Gymnodinium breve* red tide blooms: Initiation, transport, and consequences of surface circulation. *Limnol. Oceanogr*. 42, 1039-1051.

Tester, P.A., Stumpf, R.P., Vukovich, F.M., Fowler, P.K., & Turner, J.T. (1991). An expatriate red tide bloom: Transport, distribution, and persistence. *Limnol. Oceanogr*. 36, 762–767.

Tilney, C.L., Shankar, S., Hubbard, K.A., Corcoran, A.A. (2019). Is *Karenia brevis* really a low-light-adapted species? *Harmful Algae* 90, 101709, doi:10.1016/j.hal.2019.101709.

Towns, J., Cockerill, T., Dahan, M., Foster, I., Gaither, K., Grimshaw, A., *et al*. (2014). XSEDE: Accelerating scientific discovery. *Computing in Science and Engineering* 16(5), 62–74, doi:10.1109/mcse.2014.80.

Vargo, G.A. (2009). A brief summary of the physiology and ecology of *Karenia brevis* Davis (G. Hansen and Moestrup comb. nov.) red tides on the West Florida Shelf and of hypotheses posed for their initiation, growth, maintenance, and termination. *Harmful Algae* 8, 573-584.

Vargo, G. A., Heil, C. A., Fanning, K. A., Dixon, L. K., Neely, M. B., Lester, K., *et al*. (2008). Nutrient availability in support of *Karenia brevis* blooms on the central West Florida Shelf: What keeps *Karenia* blooming? *Cont. Shelf Res. 28*(1), 73–98, doi:10.1016/j.csr.2007.04.008.

Walsh, J. J., et al. (2003). The phytoplankton response to intrusions of slope water on the West Florida shelf: Models and observations. *J. Geophys. Res*. 108(C6), 3190, doi:10.1029/2002JC001406.

Walsh, J. J., Jolliff, J., Darrow, B. P., Lenes, J. M., Milroy, S. P., Remsen, D., *et al*. (2006). Red tides in the Gulf of Mexico: Where, when, and why? *J. Geophys. Res. 111*, C11003, doi:10.1029/2004JC002813.

Walsh, J.J, Weisberg, R.H., Lenes, J.M. Chen, F.R. Dieterle, D.A., Zheng, L., *et al*. (2009). Isotopic evidence for dead fish maintenance of Florida red tides, with implications for coastal fisheries over both source regions of the West Florida Shelf and within downstream waters of the South Atlantic Bight. *Progr. Oceanogr*., 80, 51-73.

Weisberg, R.H. (2011). Coastal ocean pollution, water quality and ecology: a commentary. *Mar. Technol. Soc. J.* 45 (2), 35-42.

Weisberg, R.H., & He, R. (2003). Local and deep-ocean forcing contributions to anomalous water properties on the West Florida Shelf. *J. Geophys. Res*. 108, C6, 15, doi:10.1029/2002JC001407.

Weisberg, R.H., Barth, A., Alvera-Azcárate, A., & Zheng, L. (2009a). A coordinated coastal ocean observing and modeling system for the West Florida Shelf. *Harmful Algae* 8, 585-598.

Weisberg, R.H., Liu, Y., & Mayer, D.A. (2009b). Mean circulation on the west Florida continental shelf observed with long-term moorings. *Geophys. Res. Lett.* 36, L19610, doi:10.1029/2009GL040028.

Weisberg, R.H., Zheng, L., Liu, Y., Lembke, C., Lenes, J. M., & Walsh, J.J. (2014a). Why a red tide was not observed on the West Florida continental shelf in 2010. *Harmful Algae 38*, 119–126, doi:10.1016/j.hal.2014.04.010.

Weisberg, R.H., L. Zheng, L. & Peebles, E. (2014b). Gag grouper larvae pathways on the West Florida Shelf, *Cont. Shelf Res.,* 88, 11-23, Doi:10.1016/j.csr.2014.06.003.

Weisberg, R.H., Zheng, L., & Liu, Y. (2016a). West Florida Shelf upwelling: Origins and pathways. *J. Geophys. Res. Oceans* 121, 5672-5681, doi:10.1002/2015JC011384.

Weisberg, R. H., Zheng, L., Liu, Y., Corcoran, A., Lembke, C., Hu, C., *et al*. (2016b). *Karenia brevis* blooms on the West Florida shelf: A comparative study of the robust 2012 bloom and the nearly null 2013 event. *Cont. Shelf Res. 120*, 106–121, doi:10.1016/j.csr.2016.03.011.

Weisberg, R.H., Zheng, L., Liu, Y., Murawski, S., Hu, C., & Paul, J. (2016c). Did Deepwater Horizon hydrocarbons transit to the west Florida continental shelf? *Deep Sea Res*. II, 129, 259-272, doi:10.1016/j.dsr2.2014.02.002.

Weisberg, R.H., Zheng, L., & Liu, Y. (2017). On the movement of Deepwater Horizon Oil to northern Gulf beaches. Ocean Modell., 111, 81-97, doi:10.1016/j.ocemod.2017.02.002.

Weisberg, R.H., Liu, Y., Lembke, C., Hu, C., Hubbard, K., Garrett, M. (2019). The coastal ocean circulation influence on the 2018 West Florida Shelf *K. brevis* red tide bloom. *J. Geophys. Res. Oceans* 124, 2501-2512, doi:10.1029/2018JC014887.

Weisberg, R.H., & Liu, Y. (2022). Local and deep-ocean forcing effects on the West Florida Continental Shelf circulation and ecology. *Frontiers in Marine Science,* doi:10.3389/fmars.2022.863227.

Xia, M., Mao, M., & Niu, Q. (2020). Implementation and comparison of the recent three-dimensional radiation stress theory and vortex-force formalism in an unstructured-grid coastal circulation model. *Est. Coast & Shelf Sci*. 240, 106771, doi:10.1016/j.ecss.2020.106771.

Zamudio, L., & Hogan, P.J. (2008). Nesting the Gulf of Mexico in Atlantic HYCOM: oceanographic processes generated by Hurricane Ivan. *Ocean Modelling* 21, 106–125.

Zheng, L., & Weisberg, R. H. (2012). Modeling the West Florida Coastal Ocean by downscaling from the Deep Ocean, across the continental shelf and into the estuaries. *Ocean Modell.* 48, 10–29, doi:10.1016/j.ocemod.2012.02.002.

Zhu, J., Weisberg, R.H., Zheng, L., & Han, S. (2015). On the flushing of Tampa Bay. *Estuaries and Coasts* 38, 118-131, doi:10.1007/s12237-014-9793-6.

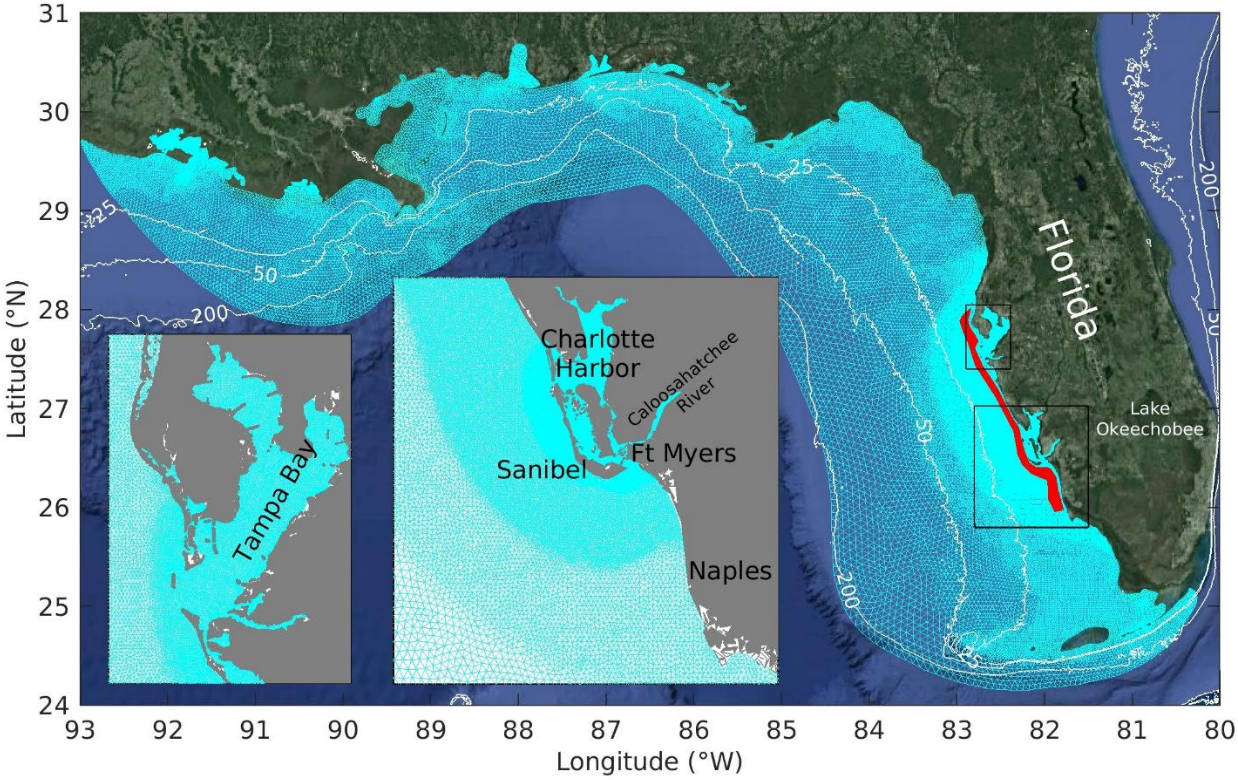

Figure 1. West Florida Coastal Ocean Model (WFCOM) domain and grid mesh (cyan). Both Tampa Bay and Charlotte Harbor regions are zoomed in as inserted maps. Also shown are tracer initiation area (red) and bathymetry contours 25, 50 and 200 m.

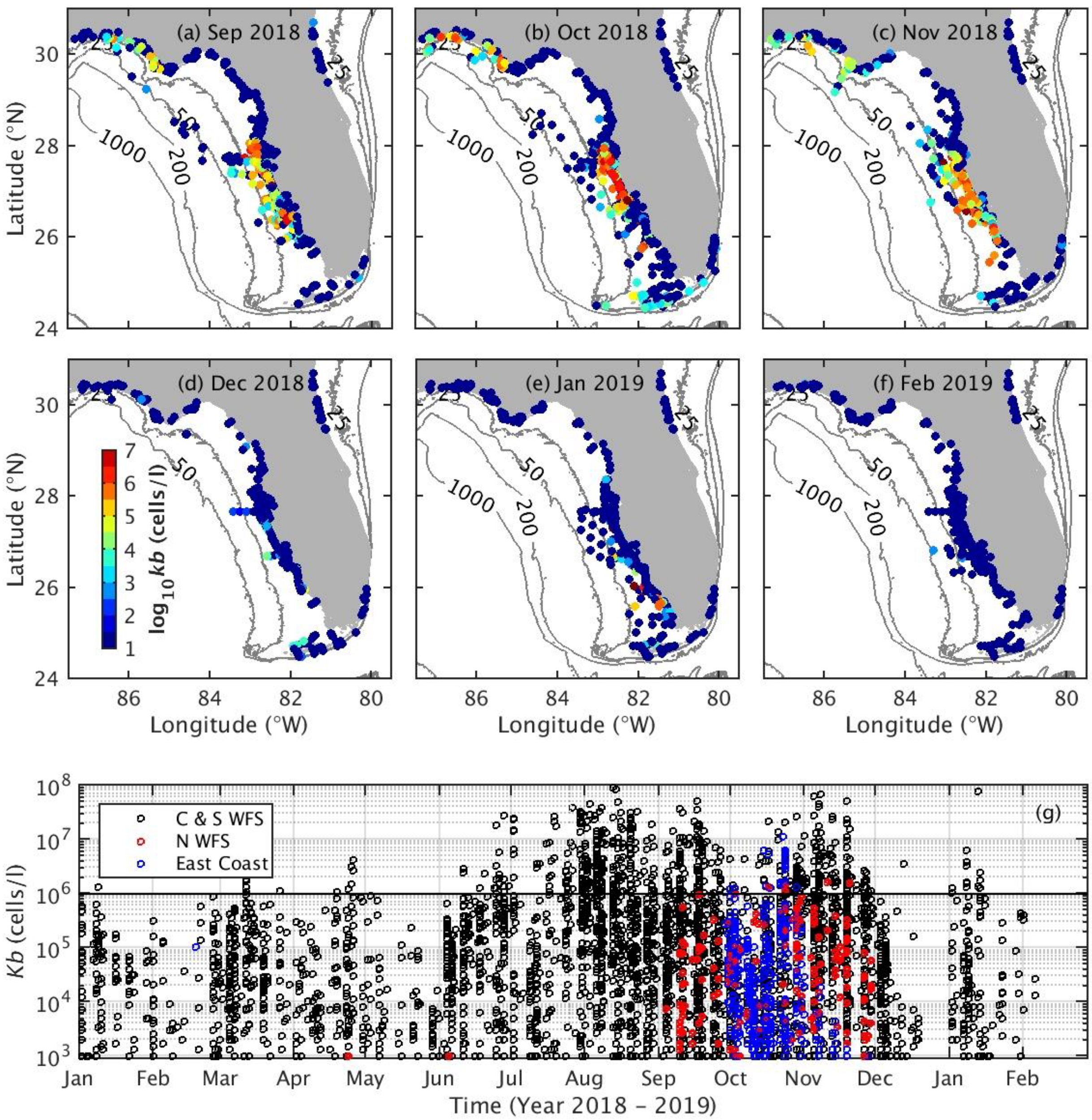

Figure 2. Monthly maps of *Karenia brevis* observations around Florida coast during September 2018 – February 2019 (a – f). The *K brevis* cell counts (cells/liter) are shown as log10 (color coded). Bathymetry units in m. Time series of the *K. brevis* bloom conditions (g) in the central and southern West Florida Shelf (WFS) coastal region (C & S WFS), the Florida Panhandle (N WFS) and on the east coast.

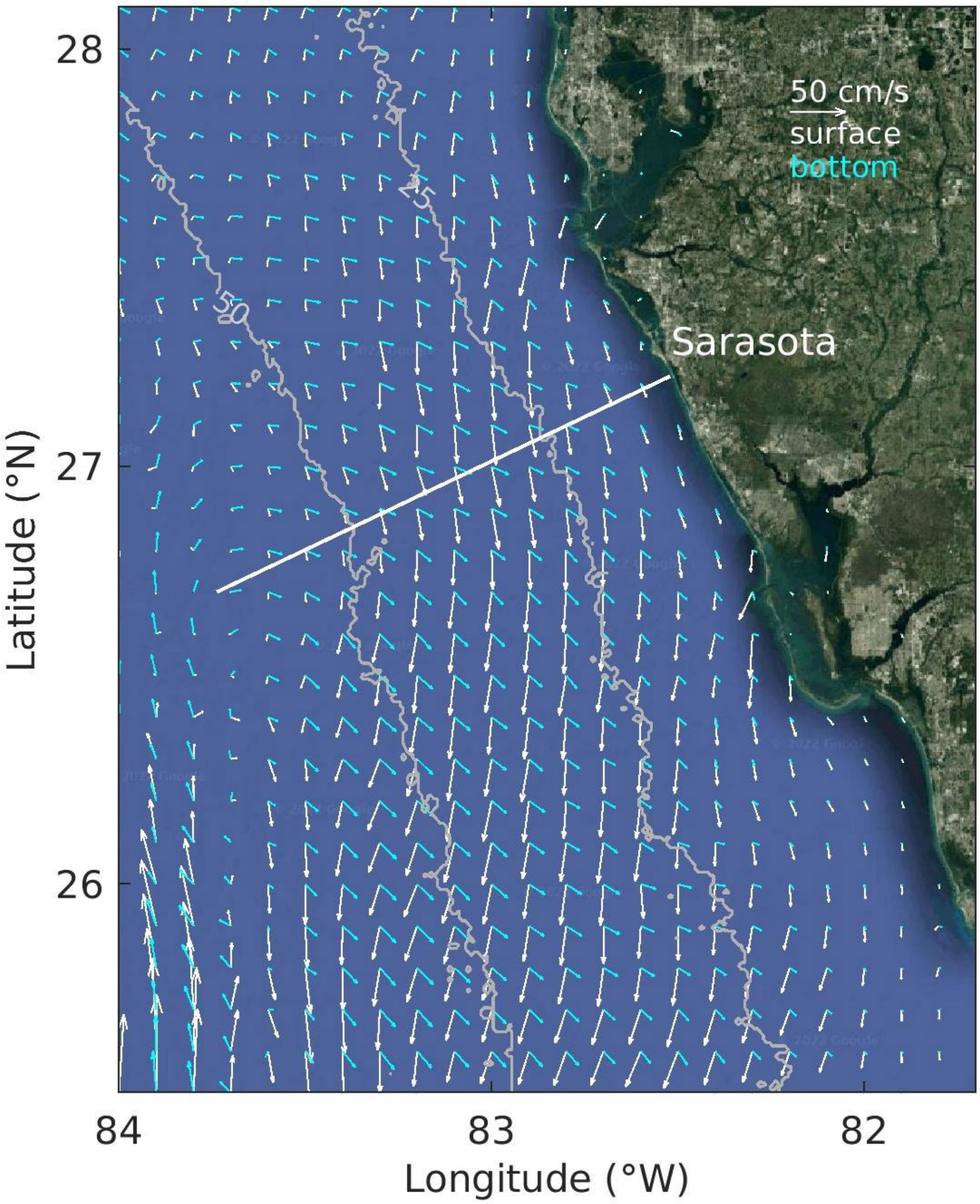

Figure 3. An example of coastal upwelling circulation pattern on the West Florida Shelf as simulated by the WFCOM for 13 October 2018. Daily averaged near surface and bottom currents are shown as white and cyan vectors, respectively. The current velocities are interpolated to a coarse rectangular grid for better visualization. The straight line shows an across-shelf transect offshore from Sarasota, Florida. Also shown are 25 m and 50 m isobaths.

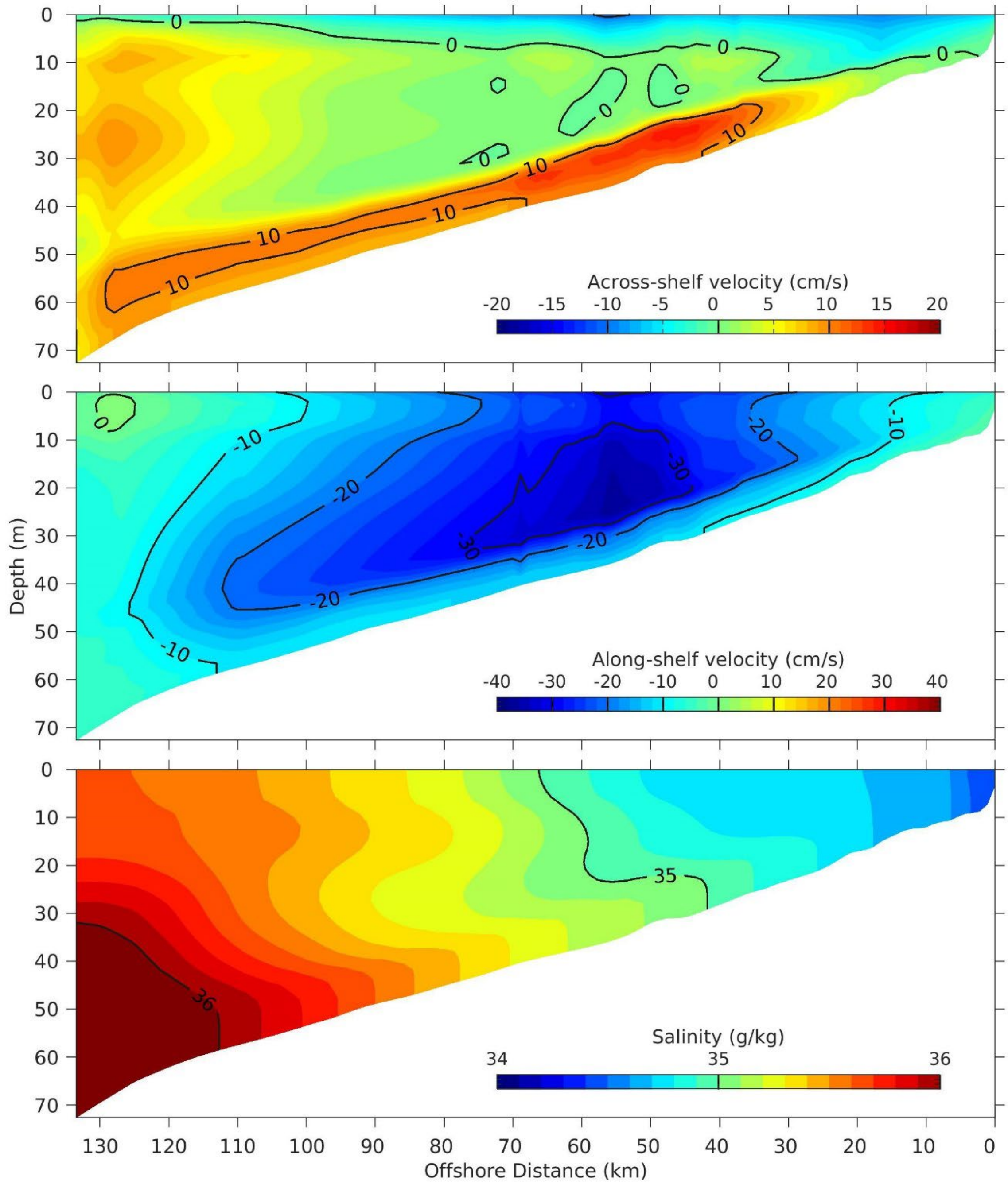

Figure 4. Across-shelf distribution of the currents and salinity in an upwelling event as simulated by WFCOM. From top to bottom, daily averaged across-shelf current velocity component (+ onshore, - offshore) and along-shelf current velocity component (+ northwestward, - southeastward) and salinity along the Sarasota transect on 13 October 2018. Note that the across-shelf velocity component shows both a bottom Ekman layer and a surface Ekman layer (top panel), and along-shelf current shows a strong coastal upwelling jet with a core at subsurface (middle panel).

675

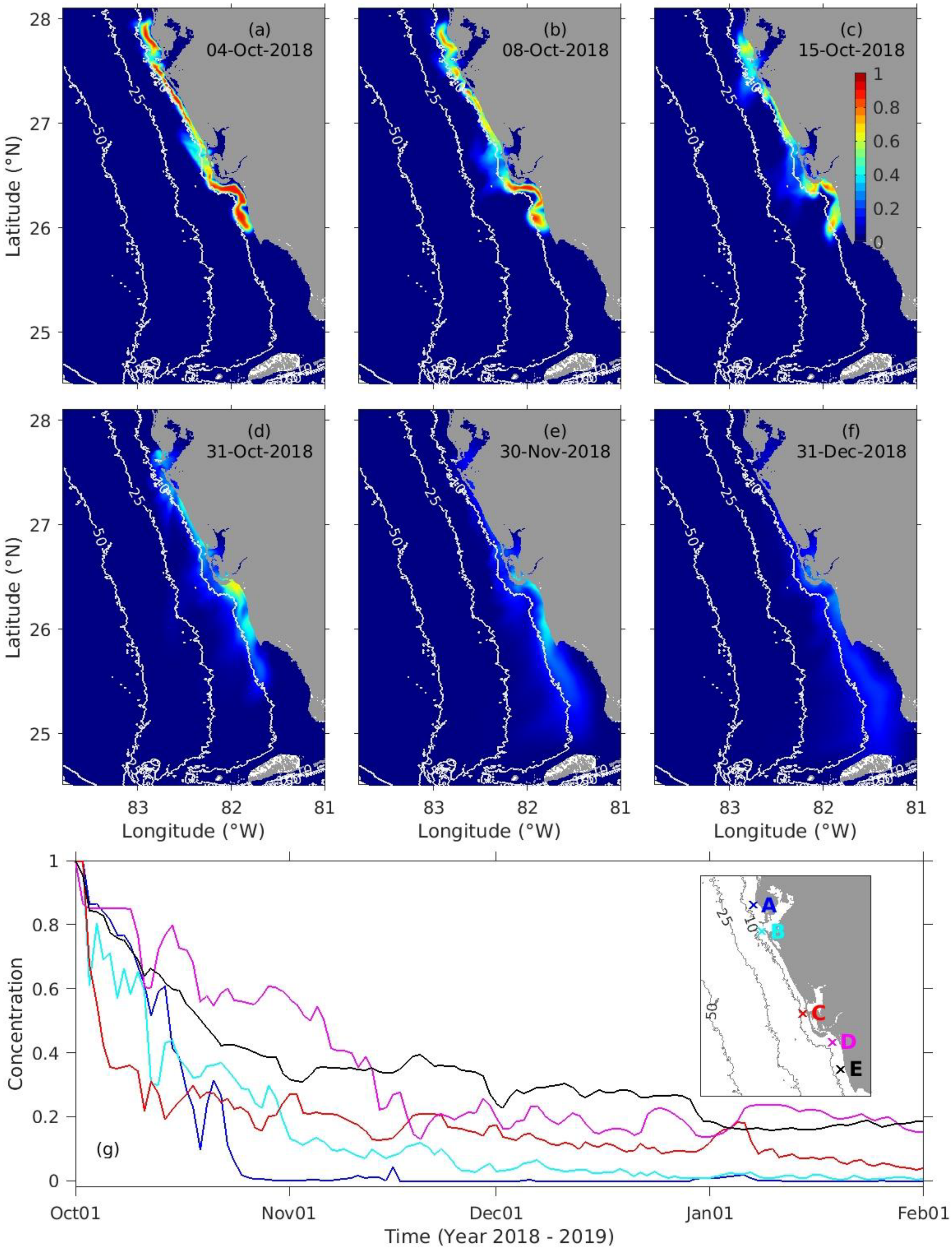

(a)
04-Oct-2018
(b)
08-Oct-2018
(c)
15-Oct-2018
(d)
31-Oct-2018
(e)
30-Nov-2018
(f)
31-Dec-2018
Latitude (°N)
Longitude (°W)
(g)
Concentration
Time (Year 2018 - 2019)
Oct01
Nov01
Dec01
Jan01
Feb01
A
B
C
D
E

Figure 5. Snapshots of model simulated surface tracer concentration for the central – south West Florida Shelf. Snapshots of surface tracer concentration three days after release (a), one and two weeks after release (b and c), and one, two and three months after release (d – f). Time series of the tracer concentration (g) sampled at five locations along the coast, from north to south, as shown in an inserted map: Clearwater coast (A), Tampa Bay mouth (B), Charlotte Harbor mouth (C), Sanibel Island (D), and Naples coast (E). Bathymetry units in m.

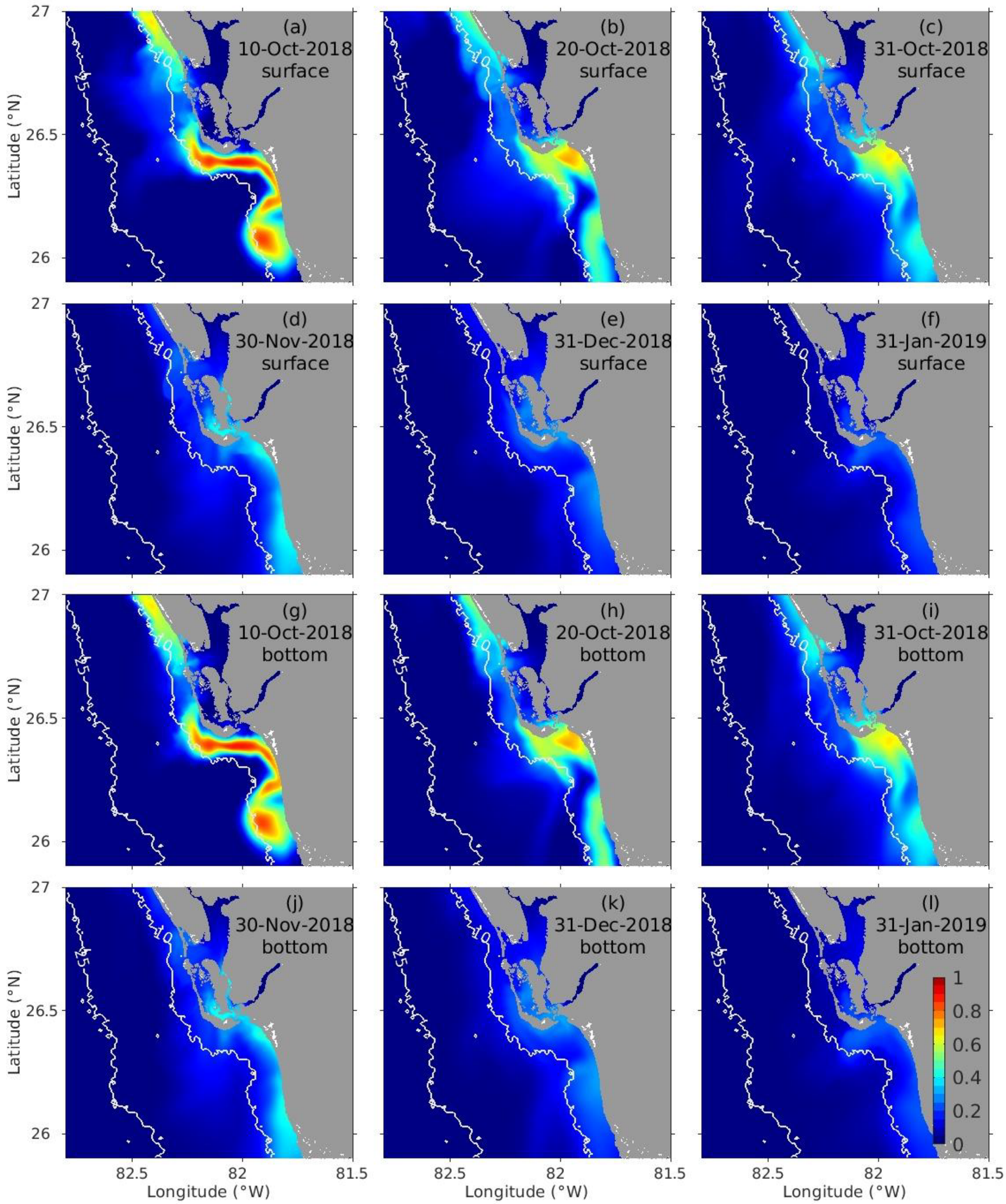

Figure 6. Snapshots of model simulated surface (top 6 panels, a – f) and bottom (bottom 6 panels, g – l) tracer concentration for Sanibel Island – Ft. Myers coastal region on 10, 20 and 31 October 2018, 30 November 2018, 31 December 2018, and 31 January 2019. Bathymetry units in m.